Neurobiology of Disease 43 (2011) 257–265

Contents lists available at ScienceDirect

Neurobiology of Disease

journal homepage: www.elsevier.com/locate/ynbdi

Natural history of disease in the YAC128 mouse reveals a discrete signature of pathology in Huntington disease

Jeffrey B. Carroll [a,1], Jason P. Lerch [c,1], Sonia Franciosi [b], Amanda Spreeuw [b], Nagat Bissada [b], R. Mark Henkelman [c], Michael R. Hayden [b,*]

[a] Centre for Molecular Medicine and Therapeutics, Child and Family Research Institute, Program in Neuroscience, University of British Columbia, Vancouver, Canada V5Z 4H4
[b] Centre for Molecular Medicine and Therapeutics, Child and Family Research Institute, Department of Medical Genetics, University of British Columbia, Vancouver, Canada V5Z 4H4
[c] The Mouse Imaging Centre, The Hospital for Sick Children, Toronto, Canada M5T 3H7

ARTICLE INFO

Article history:
Received 4 February 2011
Revised 7 March 2011
Accepted 23 March 2011
Available online 31 March 2011

Keywords:
Magnetic resonance imaging
Huntington's Disease
Mouse models
Neuropathology

ABSTRACT

Models of Huntington disease (HD) recapitulate some neuropathological features of the disease. However, a global natural history of neuroanatomy in a mouse expressing full-length huntingtin has not been conducted. We investigated neuropathological changes in the YAC128 murine model of HD using magnetic resonance imaging (MRI). Structures affected in human HD are reduced in the YAC128 mice both in absolute terms and in terms of percentage of brain volume. Structures resistant to degeneration in HD, including the cerebellum and hippocampus, are spared in the YAC128 mice. Segmentation of major white matter structures confirms specific, progressive, loss of white matter in HD. In parallel with their specific volume loss, the YAC128 mice also show progressive increases in total ventricular volume, similarly to human HD patients. Cortical atrophy in the YAC128 mice is layer specific, which is the observed pattern of cortical loss in human HD patients. Finally, we have used a classification tree analysis to maximize separation of genotypes using all 62 structure volumes in an objective manner. This analysis demonstrates that sub-cortical gray matter structures (striatum, globus pallidus, thalamus) and cerebral white matter structures (corpus callosum, anterior commisure, fimbria) are the most discriminatory. The high resolution of the current study enables robust measurement of subtle early pathological changes. The use of mice furthermore enables us to address questions difficult to address in humans, including the sequential changes of HD from baseline and the relation between MRI and stereological measures.

Introduction

Huntington disease (HD) is a neurodegenerative disorder presenting with affective, cognitive and characteristic motor symptoms (Walker, 2007). The disease is caused by a trinucleotide expansion of a cytosine–adenine–guanine (CAG) tract near the 5′ of the Huntington gene (HTT) beyond 35 repeats (The Huntington Disease Collaborative Research Group, 1993). While striatal and white matter atrophy is early and pronounced in HD (Lukes et al., 1983; Simmons et al., 1986; Harris et al., 1992; Aylward et al., 1997; Bäckman et al., 1997), other regions of the brain are also affected. Widespread loss of cortical volume has been observed in HD patient brains (Dunlap, 1927; Bäckman et al., 1997; Rosas et al., 2003). These changes are specific because cerebral atrophy occurs while cerebellar loss does not—leading to significantly altered cerebral/cerebellar ratios in adult HD patient brains (Dunlap, 1927; Rosas et al., 2003). Outside of the cortico–striatal system and cerebellum, widespread specific volume loss has been described in different areas in HD patients using MRI (Rosas et al., 2003).

Identification of pre-symptomatic HD mutation carriers has allowed investigation of brain structure before the onset of motor symptoms. Striatal volume reduction, as determined by MRI, precedes clinical onset by as much as 15 years (Aylward et al., 2004; Van Oostrom et al., 2005; Paulsen et al., 2008). Longitudinal MRI of mutation carriers demonstrates progressive ventricular enlargement and caudate atrophy (Hobbs et al., 2010a), the rate of which increases with disease burden (Hobbs et al., 2009). Less restricted global analysis of brain volume changes using voxel based morphometry reveals regionally selective, escalating atrophy in both gray and white matter in HD mutation carriers (Hobbs et al., 2010b).

The YAC128 model of HD expresses full-length mutant human huntingtin under endogenous regulatory control and accurately recapitulates many signs and symptoms of HD, including selective striatal degeneration (Slow et al., 2003; Van Raamsdonk et al., 2005d,e; Pouladi et al., 2009). Deformation-based analyses in the YAC128 mouse at 8 months of age reveal regions of shrinkage (including cortex, striatum, thalamus) as well as enlargement (including sensorimotor cortex and cerebellum) (Lerch et al., 2008b). The R6/2 mouse model, which expresses a short fragment containing exon-1 of mutant human

* Corresponding author at: 950W 28th AVE, Vancouver BC, V5Z 4H4, Canada. Fax: +1 604 875 3819.
E-mail address: mrh@cmmt.ubc.ca (M.R. Hayden).
[1] Equal contribution.
Available online on ScienceDirect (www.sciencedirect.com).

0969-9961/$ – see front matter © 2011 Published by Elsevier Inc.
doi:10.1016/j.nbd.2011.03.018

huntingtin, has also been analyzed cross-sectionally with MRI using both voxel-based morphometry (Sawiak et al., 2009a) and manual volumetry methods (Sawiak et al., 2009b). Cross sectional analyses at 18 weeks reveals that the cortex and striatum are atrophic and the lateral ventricles enlarged. Unlike human patients, who show loss of palladial volume (Rosas et al., 2003), the R6/2 mice have palladial enlargement at this stage. Longitudinal characterization of the R6/2 mice using automated morphological analysis reveals diffuse forebrain atrophy in the cerebral cortex, striatum and hippocampus that occurs at the same time (between 4–5 weeks), with approximately the same effect size, while the cerebellum is spared (Zhang et al., 2010). Surprisingly, given the widespread forebrain degeneration, the volume of the lateral ventricles shows no specific enlargement with age.

We have conducted a cross-sectional MRI-based natural history of brain structural changes in the YAC128 mouse. We used a mouse model in order to understand the complete natural history of HD, which is difficult in human patients. The extremely high resolution afforded by long *in situ* scans and genetically identical mice enables us to delineate the entire brain volume into 62 discrete structures, which empowers objective ordering of the importance of specific neuropathological changes. Furthermore, mice afford us the opportunity to make direct comparisons between MRI scans and stereological measures, definitively linking striatal atrophy to neuronal cell loss.

Results

Natural history of neuropathological changes in YAC128 mice

Total brain volume in YAC128 mice at 1 month of age (396.03 ± 4.4 mm^3) is unchanged compared to WT mice (396.61 ± 9.7 mm^3; *t*-test $t = 0.06$, $p = 0.96$). From 3 to 12 months of age, the average brain volume in the YAC128 mice is 441.2 ± 6.5 mm^3 compared to 455.2 ± 5.1 mm^3 in the WT mice (*t*-test $t(51) = 3.21$, $p = 0.0023$). This significant 3% total brain volume loss from 3 months of age is consistent with previously observed 4% total brain weight loss in the YAC128 mice at 12 months of age (Van Raamsdonk et al., 2005d) (Fig. 1A, two-way ANOVA genotype $F(1,60) = 6.03$, $p = 0.0169$).

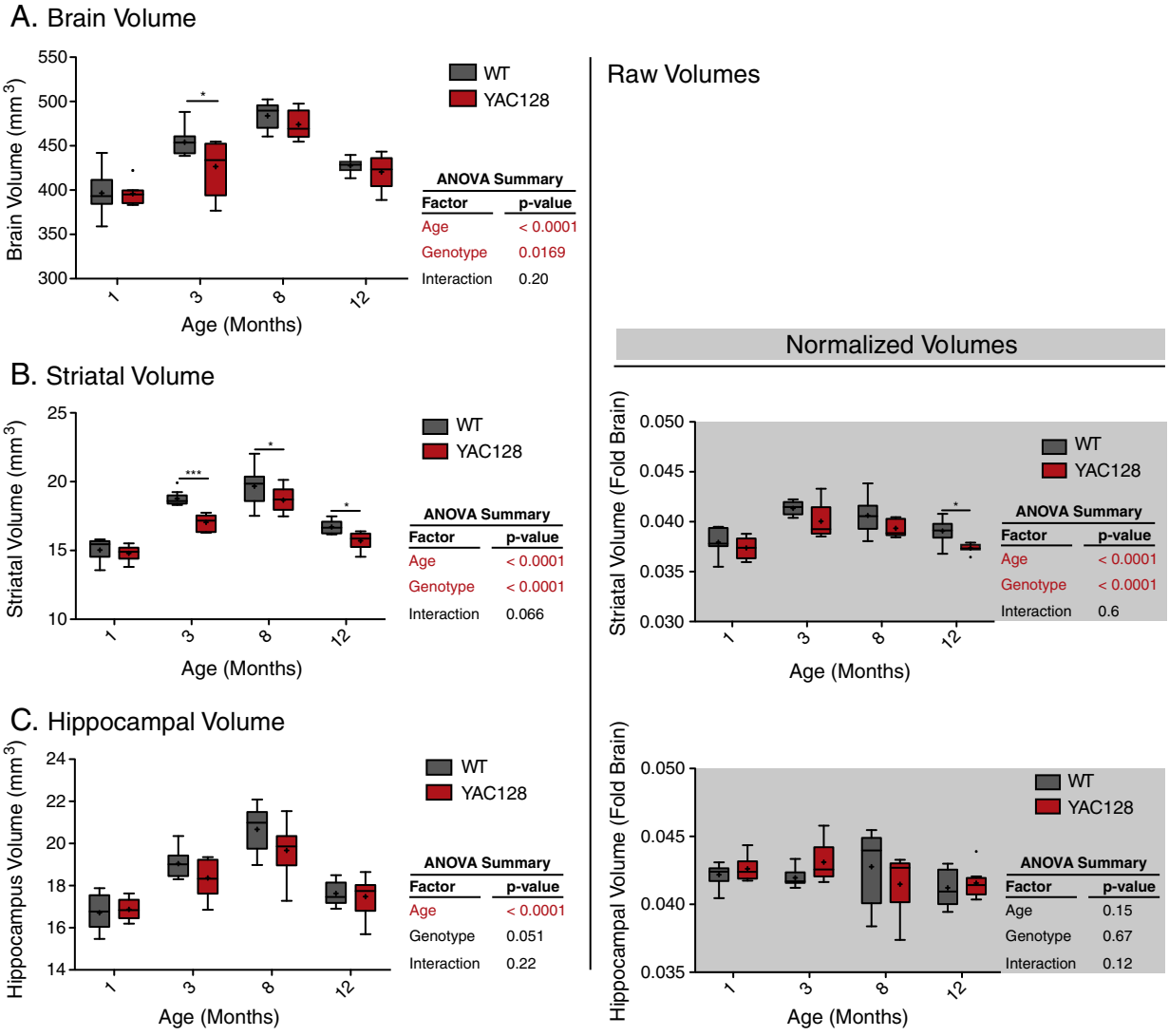

Fig. 1. Total brain volumes, as well as hippocampal and striatal volume, in aging WT and YAC128 mice. A) Total brain volume is normal in the YAC128 mice at 1 month of age, but decreased from 3 to 12 months of age (two-way ANOVA genotype $F(1,60) = 6.03$, $p = 0.0169$). B) Left—Striatal volume is normal at 1 month of age, but decreased from 3 to 12 months of age in the YAC128 mice (two-way ANOVA genotype $F(1,60) = 27.88$, $p < 0.0001$). Right—striatal volume as a percentage of total brain volume is decreased in the YAC128 mice (two-way ANOVA genotype $F(1,60) = 17.62$, $p < 0.0001$). C) Left—Hippocampal volume is normal at 1 month of age, while a trend towards decreased volume is observed from 3 to 12 months of age (two-way ANOVA genotype $F(1,60) = 3.96$, $p = 0.051$). Right—hippocampal volume as a percentage of total brain volume is unaltered in the YAC128 mice (two-way ANOVA genotype $F(1,60) = 0.19$, $p = 0.67$). $N = 1$ month (7 WT, 8 YAC128), 3 months (9 WT, 9 YAC128), 8 months (9 WT, 9 YAC128), 12 months (9 WT, 9 YAC128). Mean = "+", horizontal bars = quartiles. Post-hoc Bonferroni genotype comparisons $^{***}p < 0.001$, $^{**}p < 0.01$, $^{*}p < 0.05$.

Structure volumes can be normalized to total brain volume to correct for general brain atrophy. As previously reported (Slow et al., 2003; Lerch et al., 2008a), raw striatal volume is significantly reduced in the YAC128 mice. Using MRI we detect significant volume loss as early as 3 months of age (Fig. 1B). At 1 month of age the average YAC128 striatum is 14.8 $mm^3 \pm 0.19$ while WT striata average 15.03 ± 0.31 mm^3 (Bonferroni multiple comparison $t = 0.59$, $p > 0.05$). From 3 to 12 months of age the average YAC128 striatum is 17.2 ± 0.3 mm^3 while WT striata average 18.4 ± 29 mm^3, a decrease of 6.5% (Fig. 1B, two-way ANOVA genotype $F(1,60) = 27.88$, $p < 0.0001$).

Normalized striatal volumes, expressed as a fraction of total brain volume, show similar trends. At 1 month of age the average YAC128 striatum is 3.74% total brain volume ± 0.05% while WT striata are 3.79% ± 0.04% (Bonferroni multiple comparison $t = 0.93$, $p > 0.05$). From 3 to 12 months of age the average normalized WT striatum is 4.04% ± 0.03% total brain volume while YAC128 striata average 3.90% ± 0.03% total brain volume, a decrease of 3.5% (Fig. 1B right, two-way ANOVA genotype $F(1,60) = 17.62$, $p < 0.0001$).

The hippocampus is relatively spared in humans with early HD (Rosas et al., 2003). The size of the hippocampus shows similar decrease as total brain volume (Fig. 1C, two-way ANOVA genotype $F(1,60) = 3.96$, $p = 0.051$). However, when normalized to total brain volume, hippocampal volume is unaltered in the YAC128 mice at any time point (Fig. 1C, two-way ANOVA genotype $F(1,60) = 0.19$, $p = 0.67$).

Ventricular enlargement and cerebellar preservation

Ventricular enlargement is a prominent feature of HD neuropathology (Hobbs et al., 2010a). Raw ventricular volumes increase in aging normal mice (Fig. 2A, left, age $F(3,60) = 93.4$, $p < 0.0001$; genotype $F(1,60) = 2.37$, $p = 0.13$). Normalization of ventricular volume to total brain volume reveals increases in proportional ventricular space in the brains of YAC128 mice (Fig. 2A, right, two-way ANOVA genotype $F(1,60) = 13.25$, $p = 0.0006$). At 8 and 12 months of age the ventricles of the WT mice comprise 1.02% ± 0.017% total brain volume, while the ventricles of the YAC128 mice encompass 1.09% ± 0.018% total brain volume (*t*-test $t(33) = 2.93$, $p = 0.0062$). This 6% increase in ventricular volume is robustly detected because of the high sensitivity of our technique, with a coefficient of variation between 1.6 and 6.8% in the imaged groups.

Relative preservation of the cerebellum in adult patients with HD has long been noted (Dunlap, 1927). YAC128 transgene expression has no effect on raw cerebellar volume (Fig. 2B, left, two-way ANOVA genotype $F(1,60) = 0.04$, $p = 0.85$). When cerebellar volumes are normalized to total brain volumes, increases in cerebellar volume are observed in the YAC128 mice at 8 and 12 months of age (Fig. 2B, right, two-way ANOVA genotype $F(1,60) = 13.14$, $p = 0.0006$; genotype/age interaction $F(3,60) = 2.92$, $p = 0.041$). This demonstrates that while total cerebellar volume is unchanged in the YAC128 mice, the structure is relatively resistant to HD pathology, in agreement with observations in human patients (Rosas et al., 2003).

White matter loss—corpus callosum

White matter loss is specific and pronounced in human HD patients (Hobbs et al., 2010b). The largest brain structure comprised of predominantly white matter is the corpus callosum, and specific atrophy of the corpus callosum has been described in patients with HD (Rosas et al., 2010). At 1 month of age the volume of the corpus callosum in WT (15.91 ± 0.33 mm^3) and YAC128 (15.83 ± 0.23 mm^3) mice is equivalent (Bonferroni post-test $t = 0.15$, $p > 0.05$). From 3 to 12 months, the volume of the corpus callosum is decreased in YAC128 mice, relative to WT mice (Fig. 3A, two-way ANOVA genotype $F(1,60) = 21.08$, $p < 0.0001$; interaction $F(3,60) = 4.82$, $p = 0.0045$). The normalized corpus callosum volume was lower in YAC128 mice (Fig. 3B, two-

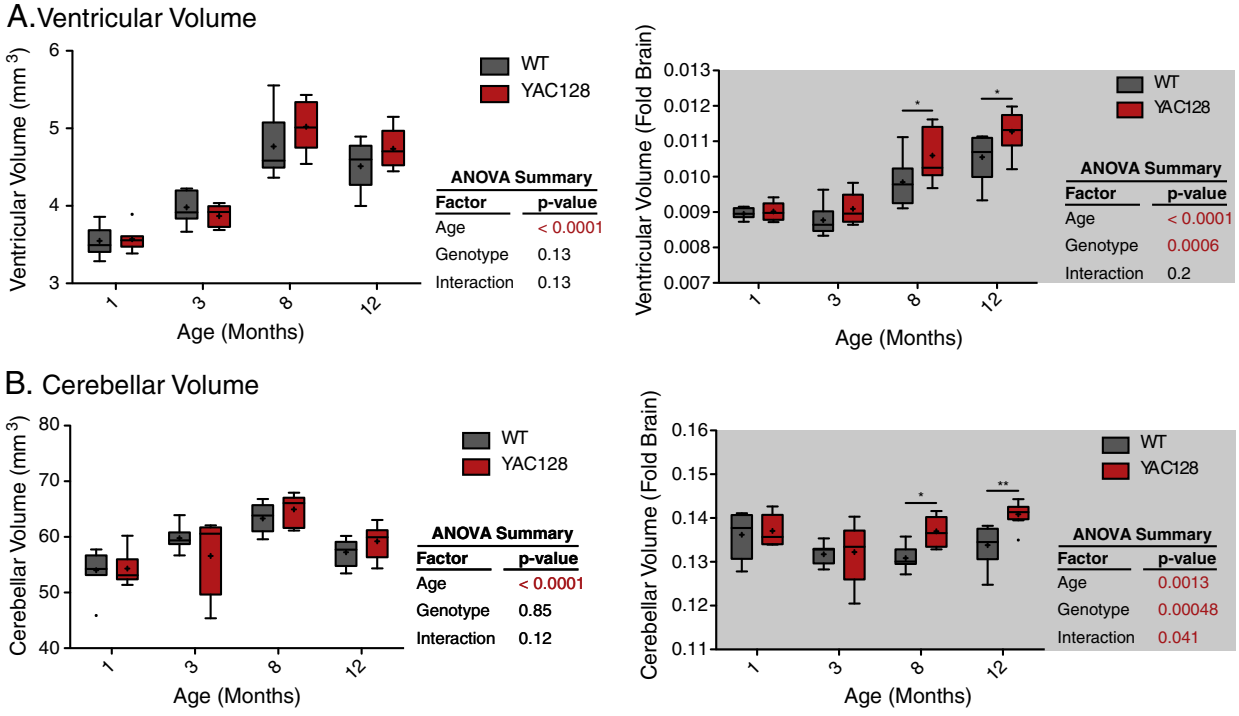

Fig. 2. Ventricular enlargement and cerebellar preservation in the YAC128 mice. A) Left—Ventricular volume increase with age, but is not significantly larger in YAC128 mice from 1 to 12 months of age (age $F(3,60) = 93.4$, $p < 0.0001$; genotype $F(1,60) = 2.37$, $p = 0.13$). Right—Ventricular volume as a percentage of total brain volume is progressively increased in the YAC128 mice (two-way ANOVA genotype $F(1,60) = 13.25$, $p = 0.0006$). B) Left—Cerebellar volume is unchanged in YAC128 mice from 1 to 12 months of age (two-way ANOVA genotype $F(1,60) = 0.04$, $p = 0.85$). Right—Cerebellar volume as a percentage of total brain volume is progressively increased in the YAC128 mice (two-way ANOVA genotype $F(1,60) = 13.14$, $p = 0.0006$; genotype/age interaction $F(3,60) = 2.92$, $p = 0.041$). $N = 1$ month (7 WT, 8 YAC128), 3 months (9 WT, 9 YAC128), 8 months (9 WT, 9 YAC128), 12 months (9 WT, 9 YAC128). Mean = "+", horizontal bars = quartiles. Post-hoc Bonferroni genotype comparisons $^{***}p < 0.001$, $^{**}p < 0.01$, $^{*}p < 0.05$.

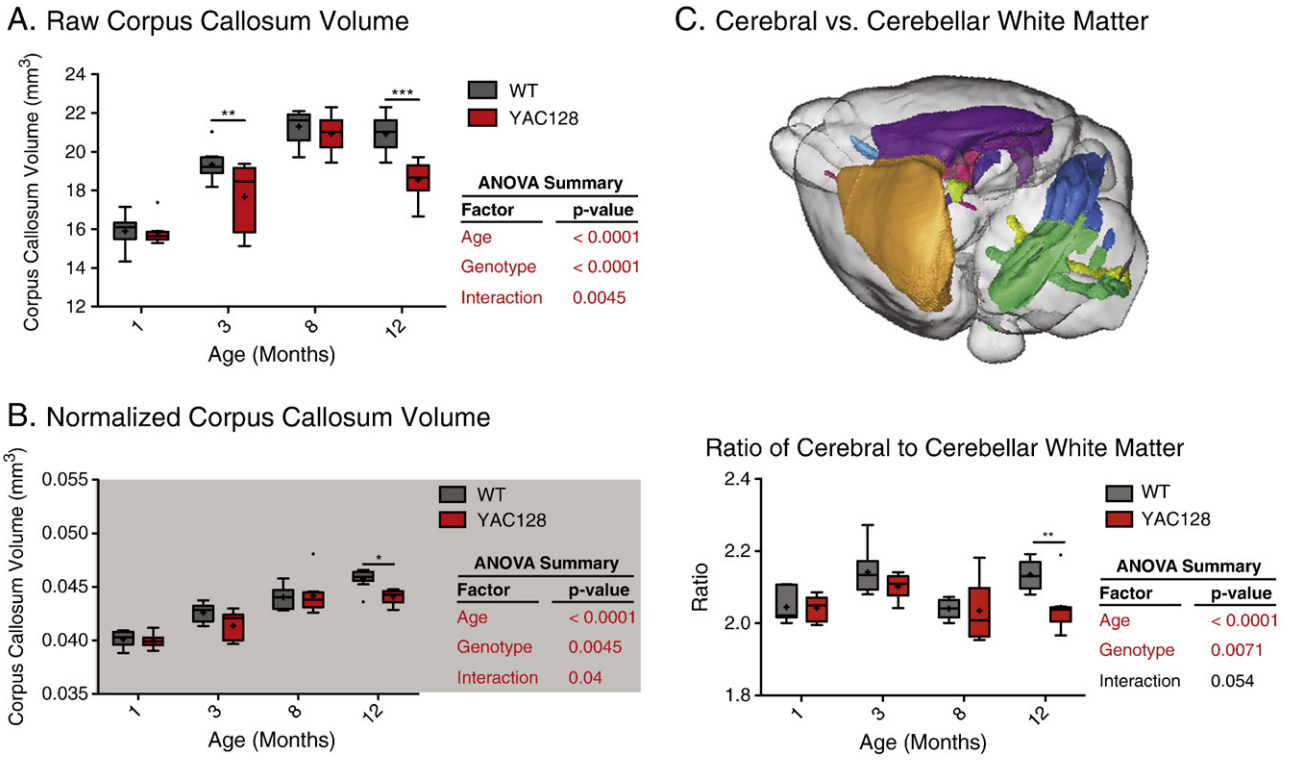

Fig. 3. Callosal atrophy in the YAC128 mice. A) The corpus callosum is normal at 1 month of age, but decreased in size between 3 and 12 months of age (two-way ANOVA genotype $F(1,60) = 21.08$, $p<0.0001$; interaction $F(3,60) = 4.82$, $p = 0.0045$). B) The corpus callosum as a percentage of total brain volume is progressively decreased in the YAC128 mice (two-way ANOVA genotype $F(1,60) = 8.72$, $p<0.0045$; interaction $F(3,60) = 3.96$, $p = 0.039$). C) Top—Sample segmentation of cerebral and cerebellar white matter (cerebral structures include the corpus callosum in orange/purple; cerebellar structures include the arbor vitea in green/blue. Bottom—The ratio of cerebral to cerebellar white matter is significantly increase in the YAC128 mice at 12 months of age (genotype $F(1,60) = 7.78$, $p = 0.0071$). $N = 1$ month (7 WT, 8 YAC128), 3 months (9 WT, 9 YAC128), 8 months (9 WT, 9 YAC128), 12 months (9 WT, 9 YAC128). Mean = "+", horizontal bars = quartiles. Post-hoc Bonferroni genotype comparisons $^{***}p<0.001$, $^{**}p<0.01$, $^{*}p<0.05$.

way ANOVA genotype $F(1,60) = 8.72$, $p<0.0045$; interaction $F(3,60) = 3.96$, $p = 0.039$).

As a further investigation of the regional specificity of pathology in the YAC128 mouse, we compared white matter loss in the cerebrum (Fig. 3C, rostral structures—corpus callosum in orange/purple) vs. the cerebellum (Fig. 3C, caudal structures, green/blue). The ratio of cerebral to cerebellar white matter is progressively reduced in the YAC128 mice (Fig. 3C, genotype $F(1,60) = 7.78$, $p = 0.0071$), confirming that the observed white matter loss is specific to the cerebrum.

Global, multivariate, signatures of pathology in the YAC128 mice

In order to objectively determine which structures maximally distinguish the YAC128 and WT mice we fit classification trees to volumes from 12-month-old mice. This determines which variables (structures) are most powerful in distinguishing levels of a factor (genotype). Maximally informative structures were then removed from the data set and the analyses re-run with the reduced set to rank the relative ability of each structure to distinguish between WT and YAC128 mice.

Table 1 presents the five most discriminatory structures in the raw and normalized data sets. In both data sets a consistent set of structures are most useful for discerning YAC128 from WT mice—particularly sub-cortical gray matter (striatum, globus pallidus and thalamus) and cerebral white matter (fimbria, corpus callosum and anterior commisure). In the normalized data set, the cerebellar cortex has high discriminatory ability based on its relative increase in YAC128 mice. These structures are in excellent agreement with human studies, which highlight many of the same regions as affected early in human HD (Rosas et al., 2003).

Stereological validation of observed early striatal atrophy

In order to validate the present findings, we performed detailed stereological determination of striatal volume of WT and YAC128 mice at 1 and 3 months of age. At 1 month of age WT striatal volume (Fig. 4A, 10.83 ± 0.4 mm^3) is equivalent to YAC128 striatal volume (Fig. 4A, 10.91 ± 0.2; t-test $t(14) = 0.20$, $p = 0.85$). By 3 months, however, YAC128 striatal volume (Fig. 4A, 12.9 ± 0.2 mm^3) is significantly lower than WT mice (Fig. 4A, 13.7 ± 0.3 mm^3, $t(59) = 2.05$, $p = 0.045$). These data demonstrate that while striatal volume loss is subtle in the YAC128 mice at 3 months of age (5.3%), it is decreased. MRI and stereological techniques are significantly

Table 1
Objective neuropathological signatures of HD in YAC128 mice.

Data	Rank	Structure	*F*-value	*p*-value	Linear model R^2
Raw	1	Striatum	13.86	0.002	0.48
Raw	2	Fimbria	9.80	0.0069	0.40
Raw	3	Corpus callosum	7.18	0.017	0.32
Raw	4	Thalamus	5.94	0.028	0.28
Raw	5	Anterior commisure (posterior)	10.89	0.0049	0.42
Norm	1	Corpus callosum	18.62	0.0006	0.55
Norm	2	Globus pallidus	22.03	0.00029	0.60
Norm	3	Striatum	15.69	0.0013	0.51
Norm	4	Cerebellar cortex	13.54	0.0022	0.47
Norm	5	Anterior commisure (posterior)	15.34	0.0014	0.51

Structures were ranked by their ability to discriminate between YAC128 and WT mice at 12 months of age using a classification tree algorithm (Breiman et al., 1984). In each data set (raw and normalized volumes) the most informative structure was identified, and a linear model constructed. The identity of the first 5 structures in each data set, along with the statistic, p-value and r^2 from the linear model for each, is reported.

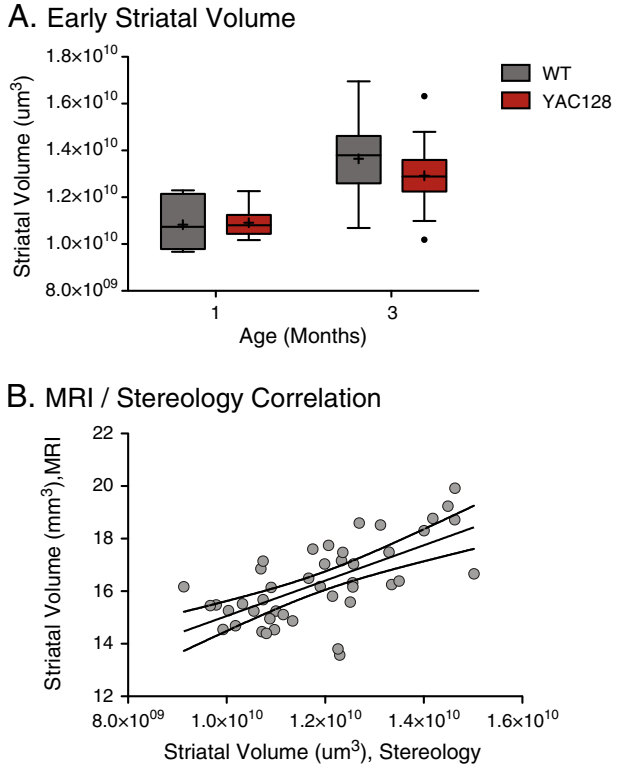

Fig. 4. Stereological validation of observed striatal volume loss. A) Striatal volume was measured using stereology at 1 and 3 months of age. Striatal volume is unchanged in YAC128 mice at 1 month of age (t-test $t(14)=0.20$, $p=0.85$), but decreased by 3 months of age (t-test $t(59)=2.05$, $p=0.045$). B) Striatal volume, as determined by stereology, is correlated with MRI-detected striatal volume ($r^2=0.44$; test of non-zero slope $F(1,42)=32.6$, $p<0.0001$). $N=1$ month (7 WT, 9 YAC128), 3 months (32 WT, 29 YAC128). Mean = "+", horizontal bars = quartiles.

correlated (Fig. 4B, $r^2=0.44$; test of non-zero slope $F(1,42)=32.6$, $p<0.0001$). The extent of the correlation ($r^2=0.44$), however, suggests that the information obtained by each technique is not identical and that they provide independently useful information.

Progressive, layer specific, cortical thinning

We have observed specific alterations in cortical thickness at 8 months of age in the YAC128 mice, particularly in the sensorimotor cortex (Lerch et al., 2008b). In an attempt to link these observations to the described sub-cortical atrophy we undertook a study of cortical neuropathology in the YAC128 mice. In human HD patients, cortical thinning is layer-specific, with projection layers III, V and VI showing more loss than non-projection layers (Hedreen et al., 1991). Based on our changes observed in our MRI studies, we analyzed cortical thickness coronal brain slices near the bregma (Lerch et al., 2008b). Layer I of the primary motor cortex, the most superficial molecular layer, is normal in the YAC128 mice at 3, 8 and 12 months of age, with a trend towards increased thickness (Fig. 5D, two-way ANOVA genotype $F(1,55)=3.07$, $p=0.085$). This same trend towards increased thickness has been observed in human HD patient brains (Hedreen et al., 1991). The granule layer, layer IV, is also unchanged in the YAC128 mice at these time points (Fig. 5D, two-way ANOVA genotype $F(1,55)=0.68$, $p=0.41$). In contrast, the superficial projection layer, layer II/III, shows significant progressive thinning at these coordinates (Fig. 5D, two-way ANOVA genotype $F(1,55)=4.24$, $p=0.044$). The deep projection layers, V/VI, are also significantly thinner in the YAC128 mice, (Fig. 5D, two-way ANOVA genotype $F(1,55)=3.2$, $p=0.077$; genotype/age interaction $F(2,55)=3.71$, $p=0.031$). These data demonstrate progressive, layer-specific, atrophy in the cortex of the YAC128 mice.

Progressive, layer specific, neuronal shrinkage and loss

In humans cortical thinning is associated with specific cortical projection neuron loss, particularly in projection layers (III and V/VI) (Hedreen et al., 1991; Heinsen et al., 1994). Using stereological techniques we counted and estimated the cross-sectional area of cortical NeuN-immunoreactive neurons in layers II/III and V/VI of WT and YAC128 mice. At 3 months of age WT mice have equivalent numbers of neurons to YAC128 mice in both layers II/III (Fig. 6A, 258 ± 9 vs. 263 ± 11 neurons/layer, respectively) and V/VI (Fig. 5E, 325 ± 9 vs. 333 ± 11 neurons/layer, respectively). By 12 months of age YAC128 mice have significantly less neurons than WT mice in both layers II/III (Fig. 6A, 269 ± 12 vs. 239 ± 11 neurons/layer, respectively, Bonferroni post-hoc $t=3.57$, $p<0.01$) and V/VI (Fig. 5F, 355 ± 15 vs. 293 ± 12 neurons/layer, respectively, Bonferroni post-hoc $t=3.58$, $p<0.01$). These data demonstrate progressive loss of cortical neurons in layers II/III (two-way ANOVA age $F(1,27)=0.36$, $p=0.55$; genotype $F(1,27)=5.27$, $p=0.03$; interaction $F(1,27)=7.1$, $p=0.013$) and V/VI (two-way ANOVA age $F(1,27)=0.18$, $p=0.67$; genotype $F(1,27)=4.70$, $p=0.04$; interaction $F(1,27)=7.9$, $p=0.009$) in YAC128 mice.

Neurodegeneration of cortical neurons may be associated with alterations in cortical neuron size. These effects could contribute to the observed thinning of the cortex of YAC128 mice (Fig. 5). Using stereological techniques, we measured NeuN-reactive cortical neuronal size in layers II/III and V/VI in WT and YAC128 mice at 3 and 12 months of age. At 3 months of age, we find equivalent size distributions in WT and YAC128 mice in both layers II/III and V/VI (Fig. 6B). By 12 months of age, we find an earlier and steeper peak in the size distribution in YAC128 mice in both layers II/III and V/VI, demonstrating a shift in the population to smaller neurons (Fig. 6B). In order to determine the significance of this loss of larger neurons we analyzed the proportion of cell soma larger than 150 μm^2 in each data set. YAC128 mice have a significantly reduced proportion of large neurons in layer V/VI and a trend towards reduction in layer II/III (layer II/III $t(28)=-1.89$, $p=0.074$; layer V/VI $t(28)=-2.07$, $p=0.047$). Thus, YAC128 mice have atrophy of the projection neuron layers of the cortex, which is associated with both shrinkage and loss of neurons.

Discussion

This study demonstrates specific recapitulation of the early human neuropathological signature of HD in aging YAC128 mice. Total brain volume is significantly reduced in the YAC128 mice from 3 to 12 months, but normal at 1 month of age. The pattern of pathology is specific, particularly once normalized to total brain volume. The basal ganglia are particularly sensitive to mutant huntingtin expression, accompanied by progressive ventricular enlargement. The cerebellum, which is uniquely preserved in human HD, is progressively enlarged, as a fraction of total brain volume, in the YAC128 mice. Careful consideration of the cortical pathology observed in the YAC128 mice demonstrates that it is regionally specific with respect to layer. This cortical pathology is associated with loss and shrinkage of neurons in projection layers and does not occur until after the development of striatal volume loss.

Global brain atrophy is a symptom of HD but is likely not the ideal target for early intervention. The most specific changes observed likely reflect the ideal targets for intervention and therefore become key endpoints in future trials. Data presented here suggests that relative striatal (Fig. 1B), ventricular (Fig. 2A), cerebellar (Fig. 2B) and white matter (Fig. 3B) volumes are progressive, highly sensitive, markers of HD pathology in the YAC128 mice. They highlight basal ganglia atrophy, as well as more widespread atrophy, which is nevertheless discrete. An important advantage of the post-mortem mouse tissue to study HD neuropathology is the high resolution achievable. Using a high field strength (7.0 T) and a long scan (~12 hours) results in voxel sizes of 0.032 mm^3 vs. 1 mm^3 voxels commonly achieved in human studies with

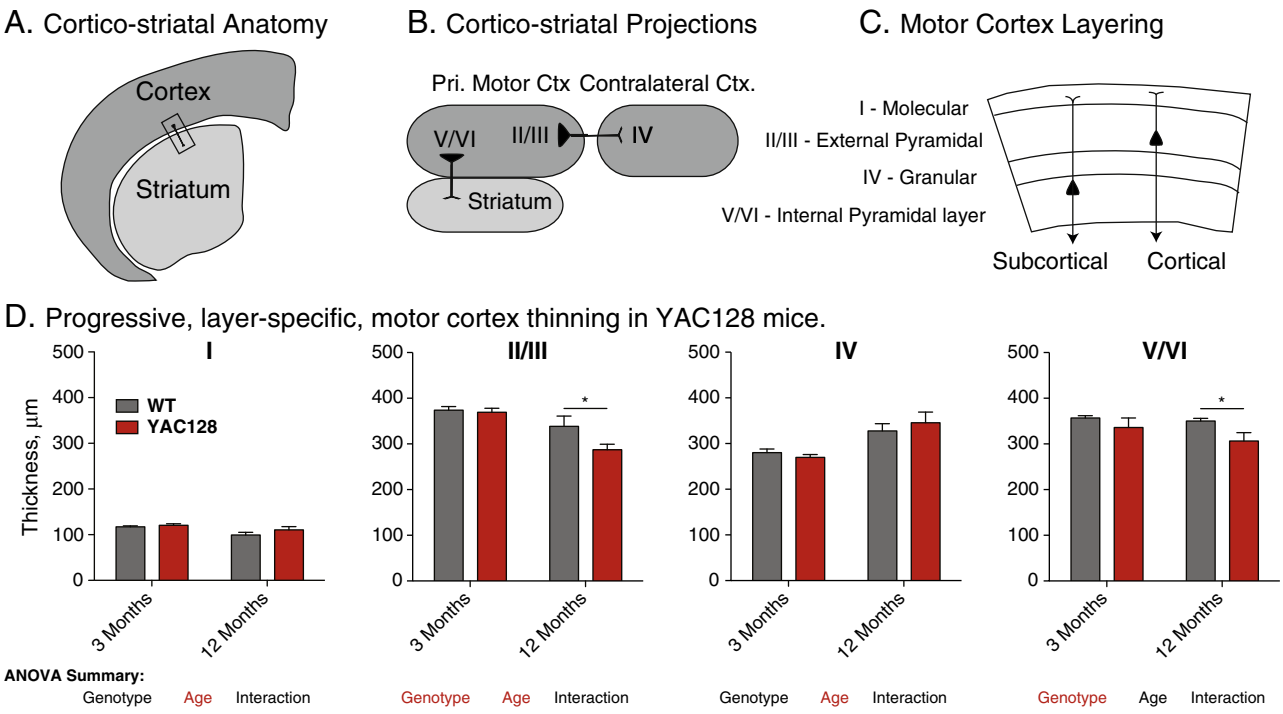

Fig. 5. Progressive, layer-specific, thinning of the primary motor cortex of YAC128 mice. A) Cartoon depicting approximate coronal sections used for analysis. B) Schematic of layer origination and termination of cortico–cortico and cortico–striatal projections. C) Layering of the mammalian cortex indicating primary projection layers (II/III and V/VI). D) Projection layers II/III and V/VI progressively thin in the YAC128 mice, while non-projection layers I and IV are unchanged from 3 to 12 months of age (layer I: two-way ANOVA genotype $F(1,55) = 3.07$, $p = 0.085$; layer II/III: two-way ANOVA genotype $F(1,55) = 4.24$, $p = 0.044$; layer IV: two-way ANOVA genotype $F(1,55) = 0.68$, $p = 0.41$; layer V/VI: two-way ANOVA genotype $F(1,55) = 3.2$, $p = 0.077$; genotype/age interaction $F(2,55) = 3.71$, $p = 0.031$). $N = 3$ months (16 WT, 14 YAC128), 12 months (8 WT, 8 YAC128). Data is graphed as mean ± SEM.

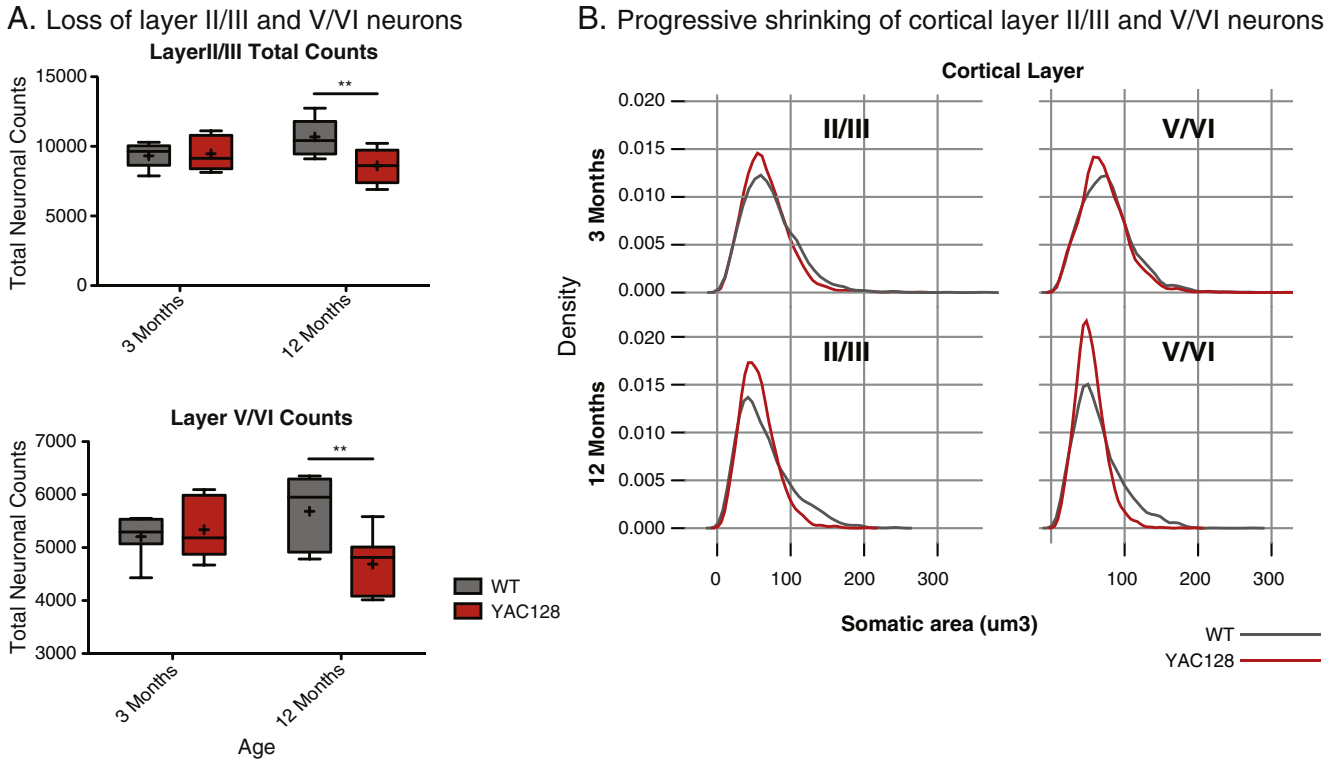

Fig. 6. Progressive loss of neurons from projection layers of primary motor cortex of YAC128 mice. A) NeuN-immunoreactive cells in layers II/III and V/VI are progressively lost from 3 to 12 months of age in the YAC128 mice. B) Density plot (smoothed histogram) of cell size distribution in the WT and YAC128 mice (gray and red lines, respectively) shows layer II/III and V/VI neuronal shrinkage from 3 to 12 months of age (linear mixed effects model layer II/III $t(28) = -1.89$, $p = 0.074$; layer V/VI $t(28) = -2.07$, $p = 0.047$). $N = 3$ months (16 WT, 14 YAC128), 12 months (8 WT, 8 YAC128). Mean = "+", horizontal bars = quartiles. Post-hoc Bonferroni genotype comparisons $^{***}p<0.001$, $^{**}p<0.01$, $^{*}p<0.05$.

1.5 T scans (Paulsen et al., 2006). This resolution allows us to delineate the entire volume of the brain into a large number of structures, providing sufficient data to objectively analyze global patterns of neurodegeneration. Choosing regions of interest invariably biases investigators towards known sites of pathology. As an example of the insights gained by this approach, we find that cerebral white matter structures are highly predictive of genotype, while cerebellar white matter structures are poor at separating WT and YAC128 mice. This confirms that the cerebellum is relatively spared in early HD and extends it by highlighting the fact that the white matter of these structures also displays regionally selective vulnerability.

Analysis of the volume of individual structures in the YAC128 mice demonstrates a dynamic pattern of degeneration. Basal ganglia structures are decreased in volume, as predicted (Fig. 1), but the onset of these changes is significantly earlier than expected (Slow et al., 2003). Striatal volume, the most widely studied endpoint in MRI studies (Slow et al., 2003; Van Raamsdonk et al., 2005a–e), decreases in the YAC128 mice between 1 and 3 months of age and remains decreased until 12 months of age. This loss of striatal volume persists after normalization for total brain size. The hippocampus is generally smaller in the YAC128 mice, in line with total brain size decreases, but its relative volume is unchanged at all time points investigated. A number of structures are similarly unaffected including the hypothalamus, medulla, olfactory bulbs and amygdala. This consideration of relative volumes reinforces the uniquely vulnerable nature of the striatum to pathological tissue loss in HD (Paulsen et al., 2008; Hobbs et al., 2010a). A number of white matter structures, including the corpus callosum, are also progressively atrophic in the YAC128 mice in relative terms (Fig. 3). White matter loss has been widely described in early stage HD patients (Rosas et al., 2003; Rosas et al., 2006; Hobbs et al., 2010b) yet has received relatively little attention in the mouse model literature. Our results suggest that white matter measures are highly specific, early and progressive and should be considered in future pre-clinical trials.

Cerebellar volume is also of interest in HD because relative sparing of the cerebellum occurs in adult human patients (Dunlap 1927; Rosas et al., 2003). The natural history provided here suggests pronounced progressive increase in the cerebellar volume in the YAC128 mice, when considered as a fraction of total brain volume. This is the clearest described mouse analog to the preservation of cerebellar volume in human HD patients. Within the CNS the cerebellum expresses the highest levels of mutant huntingtin (Strong et al., 1993; Li et al., 1993). Despite this high expression, the cerebellum is uniquely insensitive to mutant huntingtin's toxic effects. This highlights the uniqueness of HD pathology, even within the poly-glutamine disorders.

Increased total ventricular volume is obvious in human HD brains (Dunlap 1927). MRI-based investigations into both symptomatic and pre-symptomatic carriers of the HD mutation support the idea of increased ventricular volume as a very sensitive marker for the atrophy of surrounding tissue (Hobbs et al., 2010a; Paulsen et al., 2006). Processing of tissue by removal from the skull is associated with the induction of artifacts that preclude using ventricular space as a sensitive endpoint in histological trials. We find that relative ventricular size is significantly increased in the YAC128 mice, most obvious at 8 months of age (Fig. 2) validating the idea that CNS atrophy is associated with detectible ventricular enlargement. The R6/2 mice, by contrast show increased ventricular volume that does not specifically increase with time despite atrophy of the surrounding tissue (Zhang et al., 2010). The fact that striatal volume is decreased in the YAC128 mice by 3 months of age, while significant ventricular enlargement is not observed until 8 months suggests that ventricular enlargement is not due only to striatal volume loss but must originate in losses in other regions of the brain. This argues for specific early atrophy in the YAC128 mice (e.g. in the striatum), followed by more diffuse atrophy, which is apparent in increased relative ventricular and cerebellar volumes.

A crucial question about MRI in the preclinical setting is whether these studies correlate with data collected in human HD patients. Because of its unique vulnerability (Vonsattel et al., 1985; Dunlap 1927), a number of MRI studies in human patients have focused on the striatum. Striatal volume loss is more severe in human HD patients than YAC128 mice (Table 2). However, the inherent variability of human data dictates that the effect size of striatal volume loss in pre-symptomatic to early HD is comparable to 3–12 month old YAC128 mice (Table 2). These data suggest that there is an inverse relationship between severity and specificity of disease symptoms in mice.

It is critical for the prioritization of human drug trials that interventions be tested in models that accurately reflect the human condition at a given state (Table 3). As an example, excitotoxic activation of glutamate receptors has been proposed to underlie HD pathology (Fan and Raymond, 2007). Synaptic susceptibility to excitotoxicity is known to be age-dependent in both R6/2 (Cepeda et al., 2003) and YAC128 (Graham et al., 2009) mice. This suggests that anti-excitotoxic drugs should be tested in models, and at stages, in which they would be likely to help. R6/2 mice have reduced striatal spontaneous excitatory post-synaptic currents by 5 weeks of age (Cepeda et al., 2003), a time at which they begin to show diffuse forebrain atrophy (Zhang et al., 2010). Testing anti-excitotoxic compounds for effectiveness in R6/2 mice at this stage is thus likely to fail, regardless of their true efficacy and usefulness in human HD patients. By contrast, the YAC128 mice show enhanced susceptibility to excitotoxicity until 6 months of age (Graham et al., 2009). which we now show is coincident with their specific striatal volume loss (Fig. 1). More diffuse brain atrophy that we now show occurs later (Figs. 2, 3, and 6) coincides with a loss of vulnerability to excitotoxicity (Graham et al., 2009). Memantine, a non-competitive NMDAR antagonist, is effective in reducing behavioral and striatal atrophy at 12 months of age when treatment is initiated in YAC128 mice at 2 months of age (Okamoto et al., 2009). Based on our current understanding, we predict that later (i.e. "symptomatic") treatment with memantine would be unlikely to protect YAC128 mice from striatal volume changes or more diffuse brain atrophy. The appropriate advancement of pre-clinical candidates to human trials requires a deep understanding of both the targeted pathway and the pathology of the model used.

Methods

Mice

YAC128 mice (Slow et al., 2003) were maintained on the FVB/NJ strain. Each timepoint was comprised of an approximately equal number of male and female mice. Mice were genotyped and housed as

Table 2
Comparison of HD mouse model and human HD patient striatal volumes derived from MRI results.

Study	Population	Volume decrease (%)	Effect size—Cohen's d[a]
Human (Paulsen et al., 2006)	Presymptomatic	13	0.88
Human (Hobbs et al., 2010a)	At motor onset	24 (caudate)	1.9
Human (Rosas et al., 2003)	Symptomatic	33 (caudate)	2.0
Human (Rosas et al., 2003)	Symptomatic	40 (putamen)	3.6
R6/2 mice (Zhang et al., 2010)	3 months	30	9.5
YAC128 mice	1 month	1.5	0.48
YAC128 mice	3 months	3.2	0.93
YAC128 mice	8 months	3.2	0.88
YAC128 mice	12 months	4.4	1.39

Data were collected from the indicated studies and compared to YAC128 data from the current study.
[a] Cohen's d = (Control Mean − HD Mean)/Pooled Standard Deviation.

Table 3
Comparison of early vs. late MRI-detected structural changes in HD mouse models and HD patients.

Species/model	Stage	Age	Structural changes	Examples of successful interventions
R6/2 mouse (Zhang et al., 2010)	Early	4 weeks	Ventricular enlargement	Htt intrabody (Southwell et al., 2009), creatine (Ferrante et al., 2000)
R6/2 mouse (Zhang et al., 2010)	Late	12 weeks	Forebrain atrophy with cerebellar preservation	
YAC128 mouse	Early	1–3 months	Striatal volume loss, reduced brain volume	Memantine (2 months) (Okamoto et al., 2009; Milnerwood et al., 2010)
YAC128 mouse	Late	8–12 months	Ventricular enlargement, relative cerebellar preservation, relative corpus callosum loss, cortical neuronal loss	Cystamine (7 months) (Van Raamsdonk et al., 2005b)
Human HD patients	Early-Onset		Striatal volume loss	None
Human HD patients	Late-Death		Gross basal ganglia loss and ventricular enlargement, cortical atrophy, gliosis, striatal and cortical cell loss	None

Neuroanatomical changes at different stages of disease are compared between the R6/2 and YAC128 mouse models of HD, as well has human HD patients. Examples of successful therapeutic interventions at given stages are indicated.

previously described (Slow et al., 2003), and all animal experiments were conducted in accordance with protocols approved by the University of British Columbia Committee on Animal Care.

Tissue preparation and MRI acquisition

Mice were terminally anesthetized and transcardially perfused with phosphate buffered saline, followed by 4% ice-cold paraformaldehyde in PBS. Heads were removed and skulls post-fixed in 4% paraformaldehyde. Skulls were enhanced in PBS with 2 mM Prohance (Bracco Diagnostics). A 7.0 T MRI scanner (Varian Inc., Palo Alto, CA) with a 6 cm inner bore diameter insert gradient set was used for all MRI scans. Parameters used for anatomical MRI scans were: T2-weighted, 3D fast spin echo, with a TR of 325 ms, and TEs of 10 ms per echo for 6 echoes, four averages, field-of-view of $14\times14\times25$ mm^3 and matrix size of $432\times432\times780$ resulting in 0.032 mm isotropic resolution (Henkelman et al., 2006).

MRI volume segmentation

Volumes were then segmented into 62 anatomical structures using automated image registration techniques (Dorr and Lerch, 2008; Collins et al., 1995; Lerch et al., 2007). Briefly, all MRIs were aligned to a consensus space using initial linear registrations followed by iterative non-linear deformations of all images. At the end of this procedure a pre-existing atlas, wherein each voxel in the brain was assigned one of 62 anatomical structure labels, was deformed towards the consensus space of all scans in this study. Volumes were then determined by integrating the Jacobian determinant of each scan's deformation field—an index of local volume expansion or contraction—across each of the 62 anatomical structures. These methods has been validated using both simulations (Spring et al., 2007) and by comparison to stereology (Lerch et al., 2008a; Spring et al., 2010).

Immunohistochemistry

After MR acquisition 25 μm serial coronal sections were cut on a cryostat microtome (Microm Int. GmbH). Every eighth section was stained using antibody NeuN (1:1000, MAB377, Millipore). Biotinylated secondary antibodies (Vector) were used at 1:200 prior to signal amplification with an ABC Elite kit (Vector) and detection with DAB (Pierce).

Stereology

Stereology was conducted as previously described (Van Raamsdonk et al., 2005d). Briefly, the striatum was outlined and volume quantified using StereoInvestigator software (Microbrightfield Bioscience) with 8 coronal sections stained with NeuN equally spaced 250 μm apart beginning at bregma +0.02 mm. Neuronal counts and sizes were measured as described (Van Raamsdonk et al., 2005d). The thickness of each layer (I, II/III, IV and V/VI) in the primary motor cortex was with the Stereoinvestigator software "measure" tool.

Statistics

Longitudinal measures of neuroanatomical structures were considered as raw volumes, or as normalized volumes (divided by total brain volume for each mouse). Volumes were analyzed by factorial ANOVA followed by Bonferroni post-hoc tests. Two-way ANOVAs were performed using Prism 4.0 software, and density plots and classification tree analysis were done using R language and environment including the "tree" package.

Acknowledgments

This work was supported by grants from the Canadian Institute for Health Research and Michael Smith Foundation [JBC]. [MRH] is a Killam University Professor and holds a Canada Research Chair in Human Genetics and Molecular Medicine. [RMH] holds a Canada research chair in imaging technologies in human disease and preclinical models.

Appendix A. Supplementary data

Supplementary data to this article can be found online at doi:10.1016/j.nbd.2011.03.018.

References

Aylward, E.H., Li, Q., Stine, O.C., et al., 1997. Longitudinal change in basal ganglia volume in patients with Huntington's disease. Neurology 48, 394–399.
Aylward, E.H., Sparks, B.F., Field, K.M., et al., 2004. Onset and rate of striatal atrophy in preclinical Huntington disease. Neurology 63, 66–72.
Bäckman, L., Robins-Wahlin, T.B., Lundin, A., et al., 1997. Cognitive deficits in Huntington's disease are predicted by dopaminergic PET markers and brain volumes. Brain 120 (Pt 12), 2207–2217.
Breiman, J.F., Stone, C.J., Olshen, R.A., 1984. Classification and Regression Trees: Chapman and Hall/CRC, p. 368.
Cepeda, C., Hurst, R.S., Calvert, C.R., et al., 2003. Transient and progressive electrophysiological alterations in the corticostriatal pathway in a mouse model of Huntington's disease. J. Neurosci. 23, 961–969.
Collins, D., Holmes, C., Peters, T., Evans, A., 1995. Automatic 3-D model-based neuroanatomical segmentation. Hum. Brain Mapp. 3, 190–208.
Dorr, A.E., Lerch, J.P., 2008. Spring et al. High resolution three-dimensional brain atlas using an average magnetic resonance image of 40 adult C57Bl/6J mice. Neuroimage 42, 60–69.
Dunlap, C.B., 1927. Pathologic changes in Huntington's chorea with special reference to the corpus striatum. Arch. Neurol. Psychiatry 18, 867–943.
Fan, M.M.Y., Raymond, L.A., 2007. N-methyl-D-aspartate (NMDA) receptor function and excitotoxicity in Huntington's disease. Prog. Neurobiol. 81, 272–293.
Ferrante, R.J., Andreassen, O.A., Jenkins, B.G., et al., 2000. Neuroprotective effects of creatine in a transgenic mouse model of Huntington's disease. J. Neurosci. 20, 4389–4397.
Graham, R.K., Pouladi, M.A., Joshi, P., et al., 2009. Differential susceptibility to excitotoxic stress in YAC128 mouse models of Huntington disease between initiation and progression of disease. J. Neurosci. 29, 2193–2204.

Harris, G.J., Pearlson, G.D., Peyser, C.E., et al., 1992. Putamen volume reduction on magnetic resonance imaging exceeds caudate changes in mild Huntington's disease. Ann. Neurol. 31, 69–75.
Henkelman, R.M., Baghdadi, L., Sled, J.G., 2006. Presentation of 3D isotropic imaging data for optimal viewing. Magn. Reson. Med. 56, 1371–1374.
Hedreen, J.C., Peyser, C.E., Folstein, S.E., Ross, C.A., 1991. Neuronal loss in layers V and VI of cerebral cortex in Huntington's disease. Neurosci. Lett. 133, 257–261.
Heinsen, H., Strik, M., Bauer, M., et al., 1994. Cortical and striatal neurone number in Huntington's disease. Acta Neuropathol. 88, 320–333.
Hobbs, N., Henley, S., Wild, E., et al., 2009. Automated quantification of caudate atrophy by local registration of serial MRI: evaluation and application in Huntington's disease. Neuroimage 47, 1659–1665.
Hobbs, N.Z., Barnes, J., Frost, C., et al., 2010a. Onset and progression of pathologic atrophy in Huntington disease: a longitudinal MR imaging study. Am. J. Neuroradiol. 31, 1036.
Hobbs, N., Henley, S., Ridgway, G., et al., 2010b. The progression of regional atrophy in premanifest and early Huntington's disease: a longitudinal voxel-based morphometry study. J. Neurol. Neurosurg. Psychiatr. 81, 756.
The Huntington Disease Collaborative Research Group, 1993. A novel gene containing a trinucleotide repeat that is expanded and unstable on Huntington's disease chromosomes. The Huntington's Disease Collaborative Research Group. Cell 72, 971–983.
Lerch, J., Yiu, A., Bohbot, V., et al., 2007. Morris water maze training induces changes in brain shape detectable by MRI. Soc. Neurosci. 104530.
Lerch, J.P., Carroll, J.B., Spring, S., et al., 2008a. Automated deformation analysis in the YAC128 Huntington disease mouse model. Neuroimage 39, 32–39.
Lerch, J.P., Carroll, J.B., Dorr, A., et al., 2008b. Cortical thickness measured from MRI in the YAC128 mouse model of Huntington's disease. Neuroimage 41, 243–251.
Li, S.H., Schilling, G., Young, W.S., et al., 1993. Huntington's disease gene (IT15) is widely expressed in human and rat tissues. Neuron 11, 985–993.
Lukes, S.A., Aminoff, M.J., Crooks, L., et al., 1983. Nuclear magnetic resonance imaging in movement disorders. Ann. Neurol. 13, 690–691.
Milnerwood, A.J., Gladding, C.M., Pouladi, M.A., et al., 2010. Early increase in extrasynaptic NMDA receptor signaling and expression contributes to phenotype onset in Huntington's disease mice. Neuron 65, 178–190.
Okamoto, S., Pouladi, M., Talantova, M., et al., 2009. Balance between synaptic versus extrasynaptic NMDA receptor activity influences inclusions and neurotoxicity of mutant huntingtin. Nat. Med. 15, 1407–1413.
Paulsen, J.S., Magnotta, V.A., Mikos, A.E., et al., 2006. Brain structure in preclinical Huntington's disease. Biol. Psychiatry 59, 57–63.
Paulsen, J.S., Langbehn, D.R., Stout, J.C., et al., 2008. Detection of Huntington's disease decades before diagnosis: the Predict-HD study. J. Neurol. Neurosurg. Psychiatr. 79, 874–880.
Pouladi, M.A., Graham, R.K., Karasinska, J.M., et al., 2009. Prevention of depressive behaviour in the YAC128 mouse model of Huntington disease by mutation at residue 586 of huntingtin. Brain 132, 919–932.
Rosas, H.D., Koroshetz, W.J., Chen, Y.I., et al., 2003. Evidence for more widespread cerebral pathology in early HD: an MRI-based morphometric analysis. Neurology 60, 1615–1620.
Rosas, H.D., Tuch, D.S., Hevelone, N.D., et al., 2006. Diffusion tensor imaging in presymptomatic and early Huntington's disease: selective white matter pathology and its relationship to clinical measures. Mov. Disord. 21, 1317–1325.
Rosas, H., Lee, S., Bender, A., et al., 2010. Altered white matter microstructure in the corpus callosum in Huntington's disease: implications for cortical “disconnection”. Neuroimage 49, 2995–3004.
Sawiak, S., Wood, N., Williams, G., et al., 2009a. Voxel-based morphometry in the R6/2 transgenic mouse reveals differences between genotypes not seen with manual 2D morphometry. Neurobiol. Dis. 33, 20–27.
Sawiak, S., Wood, N., Williams, G., et al., 2009b. Use of magnetic resonance imaging for anatomical phenotyping of the R6/2 mouse model of Huntington's disease. Neurobiol. Dis. 33, 12–19.
Simmons, J.T., Pastakia, B., Chase, T.N., Shults, C.W., 1986. Magnetic resonance imaging in Huntington disease. AJNR Am. J. Neuroradiol. 7, 25–28.
Slow, E.J., van Raamsdonk, J., Rogers, D., et al., 2003. Selective striatal neuronal loss in a YAC128 mouse model of Huntington disease. Hum. Mol. Genet. 12, 1555–1567.
Southwell, A.L., Ko, J., Patterson, P.H., 2009. Intrabody gene therapy ameliorates motor, cognitive, and neuropathological symptoms in multiple mouse models of Huntington's disease. J. Neurosci. 29, 13589–13602.
Spring, S., et al., 2007. Sexual dimorphism revealed in the structure of the mouse brain using three-dimensional magnetic resonance imaging. Neuroimage 35, 1424–1433.
Spring, S., et al., 2010. Cerebral asymmetries in 12-week-old C57Bl/6J mice measured by magnetic resonance imaging. Neuroimage 50, 409–415.
Strong, T.V., Tagle, D.A., Valdes, J.M., et al., 1993. Widespread expression of the human and rat Huntington's disease gene in brain and nonneural tissues. Nat. Genet. 5, 259–265.
Van Oostrom, J.C.H., Maguire, R.P., Verschuuren-Bemelmans, C.C., et al., 2005. Striatal dopamine D2 receptors, metabolism, and volume in preclinical Huntington disease. Neurology 65, 941–943.
Van Raamsdonk, J.M., Pearson, J., Rogers, D.A., et al., 2005a. Ethyl-EPA treatment improves motor dysfunction, but not neurodegeneration in the YAC128 mouse model of Huntington disease. Exp. Neurol. 196, 266–272.
Van Raamsdonk, J.M., Pearson, J., Bailey, C.D.C., et al., 2005b. Cystamine treatment is neuroprotective in the YAC128 mouse model of Huntington disease. J. Neurochem. 95, 210–220.
Van Raamsdonk, J.M., Pearson, J., Rogers, D.A., et al., 2005c. Loss of wild-type huntingtin influences motor dysfunction and survival in the YAC128 mouse model of Huntington disease. Hum. Mol. Genet. 14, 1379–1392.
Van Raamsdonk, J.M., Murphy, Z., Slow, E.J., et al., 2005d. Selective degeneration and nuclear localization of mutant huntingtin in the YAC128 mouse model of Huntington disease. Hum. Mol. Genet. 14, 3823–3835.
Van Raamsdonk, J.M., Pearson, J., Slow, E.J., et al., 2005e. Cognitive dysfunction precedes neuropathology and motor abnormalities in the YAC128 mouse model of Huntington's disease. J. Neurosci. 25, 4169–4180.
Vonsattel, J.P., Myers, R.H., Stevens, T.J., et al., 1985. Neuropathological classification of Huntington's disease. J. Neuropathol. Exp. Neurol. 44, 559–577.
Walker, F.O., 2007. Huntington's disease. Lancet 369, 218–228.
Zhang, J., Peng, Q., Li, Q., et al., 2010. Longitudinal characterization of brain atrophy of a Huntington's disease mouse model by automated morphological analyses of magnetic resonance images. Neuroimage 49, 2340–2351.